Journal of Experimental Botany
doi:10.1093/jxb/erz131 Advance Access Publication 28 March 2019
This paper is available online free of all access charges (see https://academic.oup.com/jxb/pages/openaccess for further details)

RESEARCH PAPER

Maize *glossy6* is involved in cuticular wax deposition and drought tolerance

Li Li[1,2,3,*], Yicong Du[1,*], Cheng He[1,4], Charles R. Dietrich[2,†], Jiankun Li[1], Xiaoli Ma[5,‡], Rui Wang[1], Qiang Liu[2,5], Sanzhen Liu[2,4], Guoying Wang[1], Patrick S. Schnable[2,5,§] and Jun Zheng[1,§]

[1] Institute of Crop Sciences, Chinese Academy of Agricultural Sciences, Beijing 100081, P. R. China
[2] Department of Agronomy, Iowa State University, Ames, IA 50011-3650, USA
[3] Seed Science and Technology Research Center, Beijing Innovation Research Center on the Whole Process of Crop Seeds, China Agricultural University, Beijing 100193, P. R. China
[4] Department of Plant Pathology, Kansas State University, Manhattan, KS 66506, USA
[5] College of Agronomy and Biotechnology, China Agricultural University, Beijing 100193, P. R. China

* These authors contributed equally to this article.
† Present address: Monsanto, Chesterfield, MO 63005-63017, USA.
‡ Present address: Center for Plant Molecular Biology, University of Tübingen, Tübingen 72076, Germany.
§ Correspondence: zhengjun02@caas.cn or schnable@iastate.edu

Received 3 December 2018; Editorial decision 4 March 2019; Accepted 4 March 2019

Editor: Roland Pieruschka, Forschungszentrum Jülich, Germany

Abstract

Cuticular waxes, long-chain hydrocarbon compounds, form the outermost layer of plant surfaces in most terrestrial plants. The presence of cuticular waxes protects plants from water loss and other environmental stresses. Cloning and characterization of genes involved in the regulation, biosynthesis, and extracellular transport of cuticular waxes onto the surface of epidermal cells have revealed the molecular basis of cuticular wax accumulation. However, intracellular trafficking of synthesized waxes to the plasma membrane for cellular secretion is poorly understood. Here, we characterized a maize glossy (*gl6*) mutant that exhibited decreased epicuticular wax load, increased cuticle permeability, and reduced seedling drought tolerance relative to wild-type. We combined an RNA-sequencing-based mapping approach (BSR-Seq) and chromosome walking to identify the *gl6* candidate gene, which was confirmed via the analysis of multiple independent mutant alleles. The *gl6* gene represents a novel maize glossy gene containing a conserved, but uncharacterized, DUF538 domain. This study suggests that the GL6 protein may be involved in the intracellular trafficking of cuticular waxes, opening the door to elucidating the poorly understood process by which cuticular wax is transported from its site of biosynthesis to the plasma membrane.

Keywords: Cuticular waxes, drought tolerance, DUF538, glossy mutant, *glossy6 (gl6)*, maize (*Zea mays*).

Introduction

The hydrophobic cuticle covers most aerial parts of land plants and acts as a barrier to protect plants from non-stomatal water loss, ultraviolet light, physical damage caused by insects or fungi, and other biotic or abiotic stresses (Shepherd and Wynne Griffiths, 2006). The cuticle mainly consists of two types of lipophilic material, cutin and cuticular wax. Cutin is the major structural component of the cuticle and is composed of hydroxy and epoxy C_{16} and C_{18} fatty acid monomers, as well as glycerol (Nawrath, 2006). Cuticular waxes, as the second component of the cuticle, are either interspersed in the cutin

matrix (intracuticular waxes) or overlie the outermost surface of cutin polymer (epicuticular waxes). Cuticular waxes consist of complex mixtures of hydrophobic compounds, mostly very-long-chain fatty acids (VLCFAs) with more than 20 carbon atoms and their derivatives, including primary and secondary alcohols, aldehydes, alkanes, ketones, and wax esters (Lemieux, 1996; Kunst and Samuels, 2003; Samuels *et al.*, 2008). Cuticular wax composition and amounts vary greatly among plant species, tissues and organs, and development states (Lee and Suh, 2015). Primary alcohols and aldehydes are the major components of the cuticular waxes in juvenile maize leaves (Javelle *et al.*, 2010).

Cuticular wax biosynthetic pathways have been extensively studied in Arabidopsis by identification and functional characterization of wax-deficient mutant genes (Lee and Suh, 2013). The first step in wax biosynthesis is the elongation of C_{16} and C_{18} fatty acids in the endoplasmic reticulum (ER) into VLCFAs by joining C_2 building blocks of acetyl coenzyme A into a straight-chain of up to 34 carbon atoms via a fatty acid elongase complex (Samuels *et al.*, 2008; Kunst and Samuels, 2009). Following elongation, VLCFAs are modified into various wax products via the distinct alcohol-forming and alkane-forming pathways (Bernard and Joubès, 2013).

Secretion of cuticular waxes was elucidated via the identification of two membrane-located ATP binding cassette (ABC) transporters, CER5 and WBC11, responsible for wax export across the plasma membrane (PM) (Pighin *et al.*, 2004; Bird *et al.*, 2007). However, the mechanism for intracellular trafficking of wax components from their site of synthesis at the ER to the PM is less clear. Through the characterization of the Arabidopsis *ltpg* mutant, lipid transfer proteins have been proposed to be involved in cuticular wax deposition (Debono *et al.*, 2009). In addition, deficient wax secretion in mutants of the Arabidopsis *GNL1* or *ECH* genes that function in endomembrane vesicle trafficking indicated that altered ER morphology impacts wax biosynthetic capacity (McFarlane *et al.*, 2014).

In maize (*Zea mays*), our understanding of cuticular wax biosynthesis and accumulation has been aided by the identification of more than 30 glossy (*gl*) loci (Schnable *et al.*, 1994; and unpublished data from the Schnable lab), some of which have been cloned. *gl1* and *gl2*, homologs of Arabidopsis *CER3/WAX2* and *CER2*, are involved in the leaf cuticular wax alkane-forming pathway and the extension of VLCFAs to C_{30} (Tacke *et al.*, 1995; Negruk *et al.*, 1996; Hansen *et al.*, 1997; Sturaro *et al.*, 2005). *gl4* and *gl8*, homologs of *KSC6* and *KCR* of Arabidopsis, belong to the fatty acid elongase complex and play important roles in VLCFA synthesis (Xu *et al.*, 1997; Dietrich *et al.*, 2005; Liu *et al.*, 2009). *gl3* and *gl15* encode MYB and APETALA2 (AP2)-like transcription factors respectively, and both function in the regulation of cuticular wax biosynthesis (Moose and Sisco, 1996; Liu *et al.*, 2012). The *gl13* gene encodes a putative ABC transporter involved in the transport of epicuticular waxes (Li *et al.*, 2013).

One of the most important functions of plant cuticular waxes is to serve as a protective barrier against environmental stresses, including drought. Drought stress alters the composition and increases the content of cuticular waxes in Arabidopsis, rice, and wheat in some cases, and cuticular wax content has been associated with drought tolerance (Aharoni *et al.*, 2004; Kosma *et al.*, 2009; Zhu and Xiong, 2013; Zhang *et al.*, 2015). Some genes involved in biosynthesis and transport of cuticular wax may be used to improve plant drought tolerance in Arabidopsis and several crops (Lee and Suh, 2015; Xue *et al.*, 2017). However, the role of cuticular wax accumulation in drought tolerance in maize remains unclear.

Here, we report the cloning of the maize *glossy6* (*gl6*) gene that is involved in cuticular wax accumulation and show that the *gl6* mutant, relative to wild-type, exhibits reduced epicuticular wax accumulation, as well as increased cuticle permeability and seedling drought sensitivity. Further study suggests that the GL6 protein may be involved in intracellular transport of cuticular wax, providing novel insight into the cuticular wax biosynthesis/transport pathway.

Materials and methods

Plant material

The maize (*Zea mays*) *glossy6* reference mutant allele (termed *gl6-ref*, Schnable lab Ac#245) was obtained from the Maize Genetics Stock Center and maintained in the Schnable lab (Schnable *et al.*, 1994). Four additional *glossy6* alleles (*gl6-2*, *gl6-3*, *gl6-4*, and *gl6-5*) isolated via *Mu* transposon tagging screens in the Schnable lab from 1992 to 2010 were used to clone the *gl6* gene via Seq-Walking and digestion–ligation–amplification (DLA) analysis. Three ethyl methanesulfonate (EMS)-induced alleles (*gl6-6* and *gl6-7* were generated by the Schnable lab; *gl6-8* was generated by M. G. Neuffer's lab, GN) were also screened and used to verify the candidate *gl6* gene in this study (Supplementary Table S1 at *JXB* online; Schnable *et al.*, 1994).

The *gl6-ref* mutant has been backcrossed to B73 inbred line background up to eight generations and then continuously self-pollinated. BC_8F_2 segregating populations from this backcrossing program were used to map the *gl6* gene by the BSR-Seq technology, and subsequent BC_8F_3 homozygous *gl6* mutant or wild-type lines were used for the drought tolerance assay, physiology characterization, and leaf surface wax analyses.

Electron microscopy techniques

The second leaves collected from *gl6-ref* mutant and wild-type were used for field emission scanning electron microscopy (FE-SEM) analysis according to standard protocols (Aharoni *et al.*, 2004). In brief, samples were fixed on the spindle and frozen in liquid nitrogen, dried in a vacuum-drying oven and then characterized with a FE scanning electron microscope (SU8010, Hitachi, Japan).

The collected leaves were also used for transition electron microscopy (TEM) analysis by the conventional chemical protocols (Chen *et al.*, 2003). Samples were fixed in 2% glutaraldehyde in 0.1 M phosphate buffer (pH 7.4), post-fixed in 1% osmium tetroxide for 1 h, dehydrated with gradient alcohol solutions, and embedded in LR White resin. Ultrathin cross-sections were prepared with a Leica EM UC6 ultramicrotome, stained with 2% uranyl acetate for 2 h, and analysed with a transmission electron microscope (H-7500, Hitachi, Japan).

To measure the stomatal and pavement cell density and calculate the stomatal index, imprints were detached from the surface of the collected leaves and were mounted on a glass microscope slide (Nadakuduti *et al.*, 2012). Samples were observed with an optical microscope (IX71, Olympus, Japan).

Water loss and chlorophyll leaching assay

Detached leaves of the *gl6-ref* mutant and wild-type were left at room temperature and photographed and weighed every 1 h. Water loss was

calculated and represented by the percentage of fresh weight. Chlorophyll leaching assays were carried out as described (Aharoni *et al.*, 2004). Briefly, excised seedling leaves were washed with tap water, weighed, and put in 30 ml of 80% ethanol at room temperature. Four hundred microliters was removed from each sample every 10 min and used to measure the absorbance at 664 and 647 nm wavelength. Finally, the samples were incubated in boiling water, cooled on ice, and used to examine the absorbance to evaluate the total chlorophyll content. The formula in the described method was used to calculate the chlorophyll content and chlorophyll extraction rate.

Drought tolerance experiment

Seeds of the BC_8F_3 homozygous *gl6-ref* mutant or wild-type were germinated in paper towels for 2 d and then transplanted in sand-filled pots in a greenhouse (27 °C day/23 °C night, 16 h day). The control plants were well watered, and the treatment plants were subjected to drought stress by withholding water for up to 20 d, and re-watered. Six biological replications were used for this assay, and the number of surviving seedlings used to calculate the survival rate. During the drought treatment, the relative water content and relative electrical conductivity were respectively monitored by a previously described method (Zheng *et al.*, 2010). Control plants and experimental plants subjected to 10 d of drought stress were photographed. Thermal images were obtained using an infrared imaging system (VarioCam HD, InfraTec, Germany) following the manufacturer's instructions.

Analysis of wax composition

Wax extraction and gas chromatography–mass spectrometry (GC-MS) analyses were performed according to the described methods with some modifications (Chen *et al.*, 2011). The *gl6* mutant and the wild-type were grown in a substrate of roseite and sand (1:1) in a growth chamber (25 °C) under 16/8 h light/dark for three leaves (about 6–7 d after planting). Five to six grams of fresh second leaves (6 d after planting) from *gl6* mutant and wild-type seedlings were collected and immediately immersed in 5 ml chloroform for 45 s. The extracts containing 10 mg of tetracosane (Fluka) as an internal standard were transferred into opened reactive vials, dried with nitrogen gas (Pressure Blowing Concentrator; N-EVAP), derivatized by adding 20 µl of *N,N*-bis-trimethylsilyltrifluoroacetamide (Macherey-Nagel) and 20 µl of pyridine, and incubated for 40 min at 70°C. These derivatized samples were then analysed by GC with flame ionization detector (Agilent, Technologies) and GC-MS (Agilent gas chromatograph coupled to an Agilent 5973N quadrupole mass selective detector).

BSR-Seq, Seq-Walking and DLA analysis

About twenty glossy and non-glossy seedling segregants from the *gl6-ref* BC_8F_2 population were collected to construct mutant and non-mutant bulks for RNA extraction. Total RNA was isolated using the RNeasy Plus Mini Kit (Qiagen, USA) and RNA quality (RIN scores over 8) was checked on a Bioanalyzer 2100 (Agilent Technologies, USA) using an RNA 6000 Nano chip. RNA-Seq libraries were constructed using the Illumina RNA-Seq sample preparation kit according to the manufacturer's protocol. The RNA-Seq libraries were sequenced on an Illumina HiSeq2000 instrument. Sequencing data were used to perform BSR-Seq analysis following our published method (Liu *et al.*, 2012). For the Seq-Walking analysis, DNA was extracted using a cetyl trimethylammonium bromide method (Murray and Thompson, 1980) from the pools of heterozygous *B73*×(*gl6-Mu*/*gl6-ref*), in which half of the individuals contain the *Mu*-insertion allele, *gl6-2* (Supplementary Table S1). Following quantification, DNA samples were sheared using a Biorupter machine (Diagenode, USA) and sequenced. The resulting sequence data were analysed according to our published Seq-Walking strategy (Li *et al.*, 2013). DNA samples of *gl6-2* were also used to perform DLA analysis according to our published method (Liu *et al.*, 2009).

Transcriptome analysis

RNA-Seq data of the *gl6* mutant and non-mutant bulks used in the BSR-Seq analysis were also used to compare transcriptome-wide differences between the mutant and its wild-type control. Reads were aligned to the maize reference genome B73 AGPv3 using Tophat2 (Kim *et al.*, 2013). Transcript accumulation levels were calculated using the R package HTSeq (Anders *et al.*, 2015) and differentially expressed genes were identified with the R package DESeq2 (Love *et al.*, 2014). Tests for enrichment of differentially expressed genes were performed using agroGO with the standard settings (Fisher's exact test with significance threshold of 0.05, Yekutieli multi-test adjustment) (Du *et al.*, 2010).

qRT-PCR

For tissue-specific expression analysis, samples of young roots and leaves of 12 and 24 d after sowing (DAS), mature leaves of 12 and 27 d after pollination, husk, silk, anther, endosperm, embryo and seeds of 14 and 27 d after pollination were collected from the inbred line B73, and then were used to extract total RNAs by TRIzol reagent (Invitrogen). Quantitative real-time RT-PCR (qRT-PCR) analysis was conducted with TransStart Green qPCR SuperMix (TransGen Biotech) on a 7300-sequence detection system (Applied Biosystems). Maize *actin1* was used as internal control, and the relative expression of *gl6* mRNA was calculated using the $2^{-\Delta\Delta Ct}$ method (Livak and Schmittgen, 2001).

Subcellular location of GL6

To generate a GL6–yellow fluorescent protein (YFP) fusion construct, the open reading frame (ORF) of the *Gl6* gene was cloned into the pEarleyGate-101 vector that contains the YFP reporter gene (Earley *et al.*, 2006). Using previously described polyethylene glycol (PEG)-mediated transformation protocols (Chen *et al.*, 2014), the GL6–YFP construct was transformed into maize protoplasts alone or co-transformed with an ER marker (red fluorescent protein (RFP)–CNX), a Golgi marker (mRFP–ManI), a *trans*-Golgi network (TGN) marker (RFP–SYP41), or a nuclear protein marker (mRFP–AHL22) (Xiao *et al.*, 2009; Cui *et al.*, 2014). Fluorescence signals were observed under a confocal laser scanning system (Leica Microsystems, Wetzlar, Germany).

Accession numbers

Sequence data from this article can be found in the GenBank/EMBL databases under the following accession numbers: GL6 (GRMZM2G139786). The accession numbers for proteins in the phylogenetic analysis are gi 670387534, gi 1162441486, gi 241943026, gi 514753272, gi 1238298764, gi 1070905880, gi 573963963, gi 125537042, gi 77556167, gi 222626102, gi 357161708, gi 1149739371, and gi 474448180.

Results

Morphological and biochemical characterization of the gl6 *mutant*

The spontaneous *gl6* mutant first described by Emerson in 1935 has been designated *gl6-ref* (Emerson *et al.*, 1935, Schnable *et al.*, 1994). Like other glossy mutants in maize, seedling leaves of the *gl6-ref* mutant are shiny green in appearance, and water droplets easily form and adhere to leaf surfaces after leaves are sprayed with water (Fig. 1A). The accumulation of epicuticular waxes on the second leaf surface of the *gl6-ref* mutant was examined via FE-SEM. Substantially fewer wax crystals were observed on surfaces of *gl6-ref* mutant leaves relative to surfaces of wild-type leaves (Fig. 1B). Ultrastructural analysis of leaf epidermal cells by TEM found that *gl6-ref* epidermal cells contained irregular masses in the vacuole, which were absent

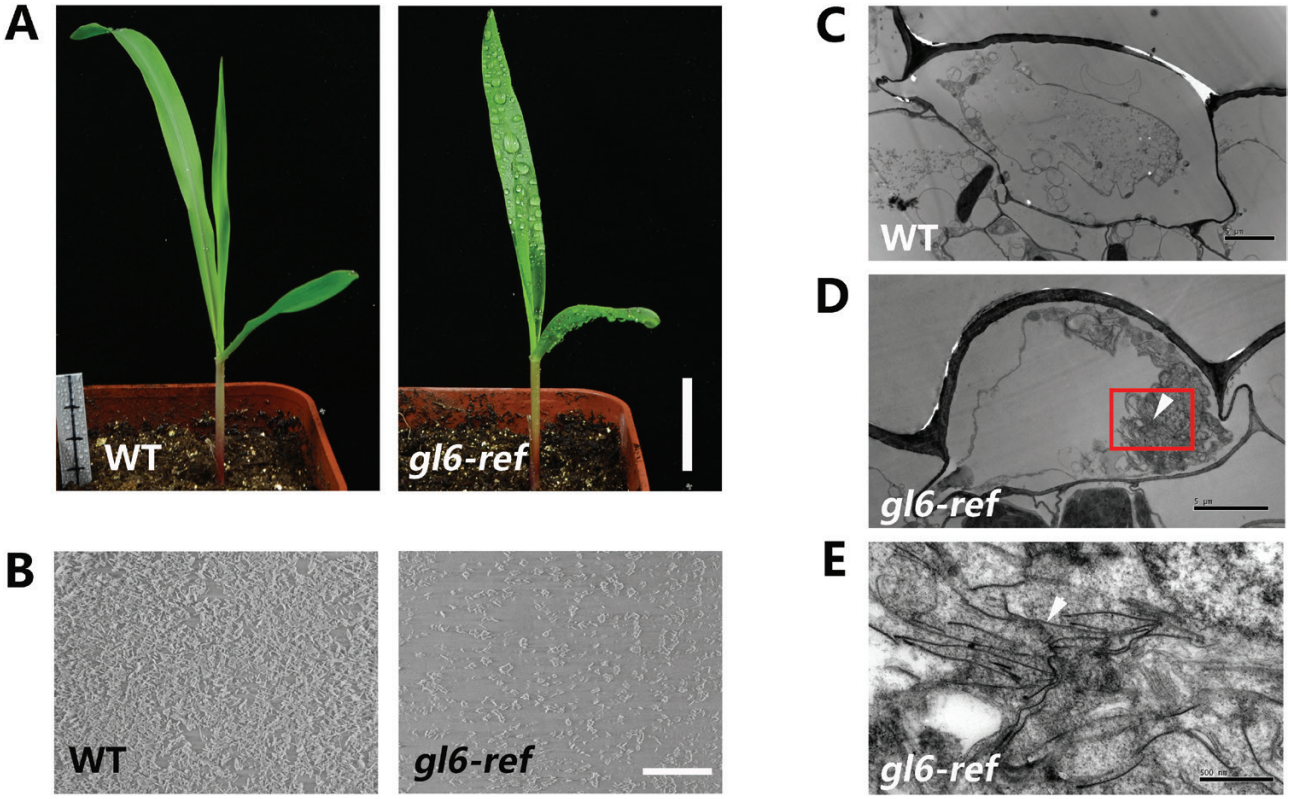

Fig. 1. Morphological characterization of the *gl6-ref* mutant. (A) *gl6-ref* mutant exhibits a glossy phenotype. Water is sprayed on seedlings to distinguish *gl6-ref* mutant seedlings from wild-type (WT). (B) Adaxial leaf epicuticular wax accumulation in WT and mutant (*gl6-ref*) seedlings detected via SEM. ×5000 magnification. (C–E) TEM analysis of leaf epidermal wax secreting cells from WT and *gl6-ref* mutant. (E) Enlarged view showing the red rectangular area marked in (D). Arrows in (D, E) indicate unusual linear inclusions. Scale bars: 3 cm in (A), 5 μm in (B–D), 500 nm in (E). (This figure is available in color at *JXB* online.)

from the wild-type cells (Fig. 1C, D). Within the masses, linear inclusions were found only in epidermal cells of the *gl6-ref* mutant (Fig. 1E). Other than this, no significant differences were observed between the two genotypes including cuticle morphology and the epidermal cell wall. This finding is similar to the observation of linear inclusions in Arabidopsis *cer5* mutants, which exhibit defects in export of waxes through the PM (Pighin *et al.*, 2004). Our results, therefore, suggested that waxes have accumulated within *gl6* cells.

The wax load and composition of the *gl6-ref* mutant were assessed via GC-MS. Relative to wild-type, leaf surface wax loads on the *gl6* mutant were reduced by 80%, from the wild-type level of 13.2 μg cm^{-2} to 2.6 μg cm^{-2} (Fig. 2A). Wax composition analysis showed that aldehydes and primary alcohols were highly reduced in the *gl6* mutant, which decreased to 1.5% and 22% of wild-type levels, respectively. In addition, the accumulations of fatty acids, alkanes, ethyl stearate, β-sitosterol, and several unidentified wax classes were also decreased in the *gl6* mutant (Fig. 2B). For individual wax constituents, amounts of C_{32} aldehydes and C_{32} primary alcohols on *gl6* mutant leaves were significantly less than on wild-type leaves. Amounts of C_{18}, C_{31} fatty acids, C_{29}, C_{31}, C_{32} alkanes, C_{30}, C_{34} aldehydes and C_{30}, C_{33} primary alcohols were also reduced in the *gl6* mutant (Fig. 2B). The compounds with reduced accumulation in the *gl6* mutant are those having chain lengths of 29 or more carbons, with the exception of C_{18} fatty acids. This suggests that *gl6* has its main impact on the accumulation of VLCFAs and their derivatives.

We further quantified total waxes including both surface and intracellular waxes and determined the proportion of total waxes secreted to the surface. This experiment was performed according to published methods (McFarlane *et al.*, 2014). Briefly, two separate approaches were used to collect (i) leaf surface waxes, representing epicuticular waxes, and (ii) leaf total waxes, including both surface/epicuticular and intracellular waxes. Surface waxes were extracted through brief dipping of plant leaves in chloroform. In contrast total waxes were extracted by homogenizing leaves in chloroform. Extracted waxes were quantified via GC-MS. As a result, total waxes were reduced from the wild-type level of 19.7 μg cm^{-2} to 13.1 μg cm^{-2} in the *gl6* mutant (Table 1). In wild-type leaves, 67.1% of total waxes were from surface waxes, suggesting that most waxes were secreted (Table 1). In contrast, only 19.9% of total waxes were surface waxes in mutant leaves. In conjunction with the observation of linear inclusions in *gl6* epidermal cells (Fig. 1D, E), these results suggest that the wax exporting system is dysfunctional, causing a large proportion of waxes to remain within epidermal cells. Taken together, these results indicated that *gl6* is involved in both the biosynthesis of very-long-chain waxes, particularly C_{32} aldehydes and C_{32} primary alcohols, and, possibly, wax transport from the ER to the plant surface.

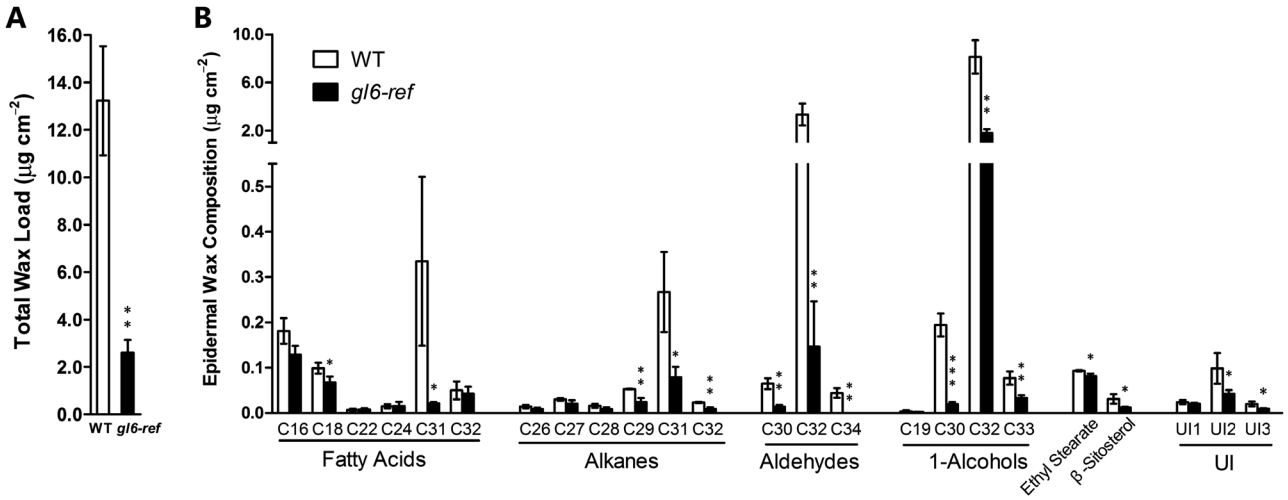

Fig. 2. Total leaf epicuticular wax load and wax composition of wild-type and *gl6-ref* mutant. (A) Total leaf cuticular wax load of wild-type and *gl6-ref* mutant. (B) Epicuticular wax composition of wild-type and *gl6-ref* mutant. Values are means of eight biological replicates ±SD. UI, unidentified. Asterisks indicate statistically significant differences between wild-type and *gl6-ref* mutant (*P<0.05, **P<0.01, ***P<0.001, Student's t-test).

Table 1. *Epicuticular wax extracted from the leaf surface compared with total wax of wild-type and* gl6 *mutant*

Parameter	WT	*gl6-ref*
Total wax (μg cm^{-2})	19.7±4.1	13.1±2.4
Surface wax (μg cm^{-2})	13.2±2.3	2.6±0.5
Wax secretion ratio	67.1%	19.9%

Total wax extraction and calculation of ratio of wax secretion were performed following a reported measurement strategy (McFarlane *et al.*, 2014). Total and surface wax content are means ±SD.

Increased cuticle permeability and drought sensitivity of the gl6 *mutant*

Reduced cuticular wax accumulation is associated with increased cuticle permeability (Kerstiens, 1996; Aharoni *et al.*, 2004; Bessire *et al.*, 2007). We performed chlorophyll leaching and water loss assays using seedling leaves of *gl6-ref* mutant and wild-type plants. For the chlorophyll leaching assay, the concentration of leaf chlorophyll in the solution was monitored at various time points. The results showed that leaf chlorophyll leaching of the *gl6-ref* mutant was faster than that of wild-type (Fig. 3A), even though the total leaf chlorophyll contents of the *gl6-ref* mutant and wild-type were similar (Fig. 3B). To detect water loss, detached leaves of *gl6-ref* and wild-type were exposed to air at room temperature; *gl6-ref* mutant leaves were obviously curled and wilted after only 2 h (Fig. 3C). The rate of water loss of detached leaves from the *gl6-ref* mutant was significantly higher than that of wild-type (Fig. 3D). Results from both the chlorophyll leaching and water loss assays suggested that *gl6-ref* mutant leaves exhibit increased cuticle permeability as compared with wild-type leaves.

Leaf water loss has been associated with reduced leaf surface temperature, and hence monitoring leaf surface temperature is widely used as an indicator of leaf water loss (Mustilli *et al.*, 2002). The surface temperature of *gl6-ref* mutant leaves, monitored via infrared thermography, was lower than that of wild-type leaves under both drought stress and well-watered conditions (Fig. 4A), while stomatal density, pavement cell density, and stomatal index of the *gl6-ref* mutant were similar to those of wild-type (Fig. 4B–D). These results suggested that the decreased leaf wax accumulation of the *gl6-ref* mutant caused faster water losses.

Given the increased cuticular permeability and leaf water loss of the *gl6-ref* mutant, we investigated how *gl6-ref* mutant seedlings respond to drought stress. As a result, under severe drought stress, the *gl6-ref* mutant showed a more severe wilting phenotype as compared with wild-type controls (Fig. 4E), and after re-watering, about 50% of wild-type seedlings could recover and survive, whereas none of the *gl6-ref* mutant seedling plants could survive (Fig. 4E, F). Under the well-watered conditions, no significant phenotypic differences in either the wilting phenotype or the relative water content of leaves were observed between *gl6-ref* mutant and wild-type seedlings (Fig. 4E, G). In contrast, under mild drought stress, the relative water content of *gl6-ref* mutant seedling leaves was lower than that of wild-type controls, 53.0% in *gl6-ref* as compared with 72.3% in wild-type. The re-watering plants after drought stress showed no significant differences in the leaf relative water content between two genotypes (Fig. 4G). In addition, a leaf electrolyte leakage assay for evaluating membrane damage was conducted, and the results showed that, under mild drought stress, the *gl6-ref* mutant exhibited an electrical conductivity of 35.1%, higher than the value of 18.2% of wild-type (Fig. 4H), which indicated that a larger degree of membrane damage in the mutant resulted in higher electrolyte leakage. In re-watered plants, no significant differences of the relative conductivity were observed between mutant and wild-type (Fig. 4H). The results corroborated that the *gl6-ref* mutation reduced seedling tolerance to drought.

Molecular cloning of gl6

Previously, the *gl6* gene had been mapped roughly to the long arm of chromosome 3 (Schnable *et al.*, 1994). BSR-Seq,

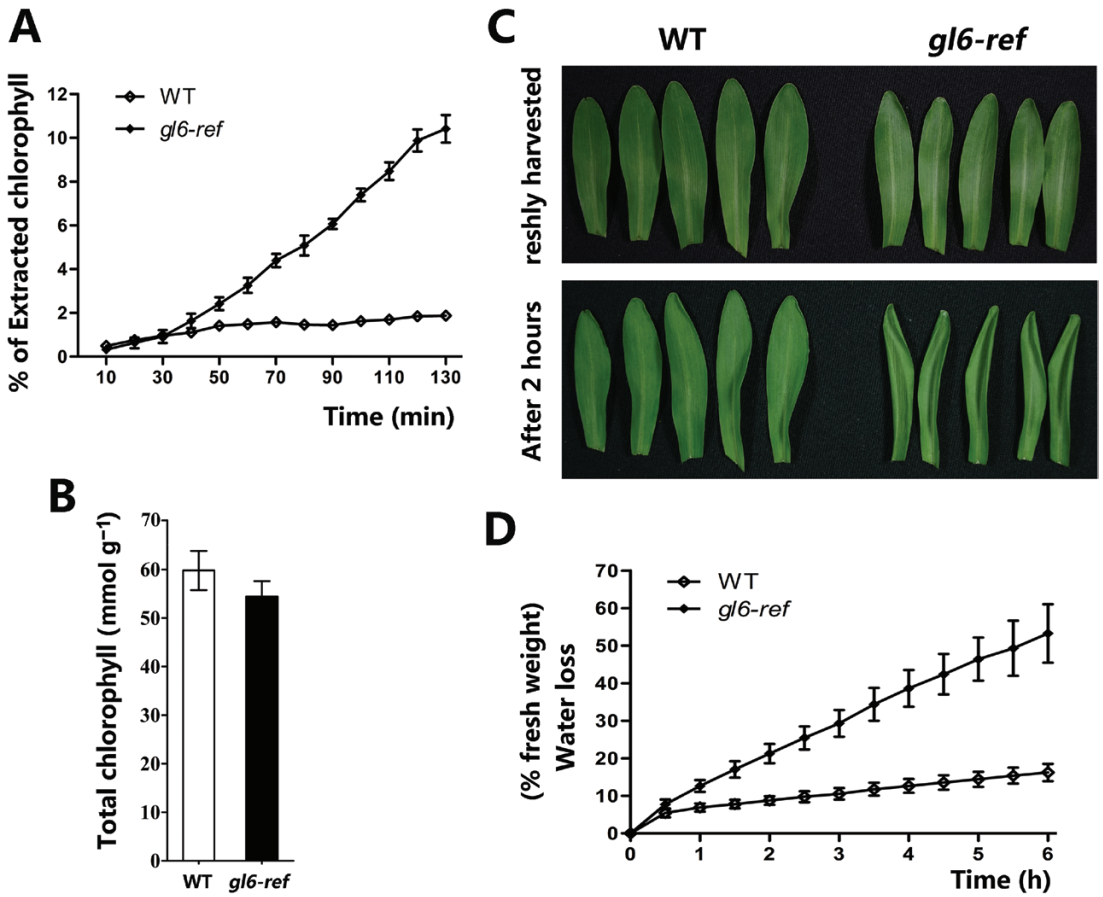

Fig. 3. Leaf surface permeability analysis of *gl6-ref* mutant. (A) Kinetics of chlorophyll leaching from leaves of the WT and *gl6-ref* mutant. (B) The total leaf chlorophyll content of WT and *gl6-ref* mutant. (C) Detached leaves from WT and *gl6-ref* mutant immediately after harvest and after 2 h at room temperature. (D) Water loss of detached leaves of the WT and *gl6-ref* mutant. Values in (A, B, D) are means of three biological replicates ±SD. (This figure is available in color at *JXB* online.)

a method utilizing RNA-Seq for bulked segregant analysis (Liu *et al.*, 2012), was performed to map the gene. Briefly, segregating BC_8F_2 populations derived from self-pollination of *gl6-ref* heterozygous plants were used to identify and collect mutant and wild-type plants, separately pooled into two bulks for RNA extraction and sequencing. Three replicates were conducted, producing six RNA-Seq datasets, each of which had more than 20 million reads. RNA-Seq reads were aligned to the B73 reference genome (AGPv2), and the polymorphic single nucleotide polymorphisms identified were used as genetic markers to map the target gene. Through this process, the *gl6* gene was mapped to an 18.9 Mb interval on chromosome 3, from 113.5 to 132.4 Mb (Fig. 5A).

To facilitate the identification of the *gl6* gene, additional *gl6* alleles were generated through *Mu* transposon mutagenesis and chemical (EMS) treatment (Candela and Hake, 2008). Four new *Mu*-tagged alleles were identified in the progeny of crosses between homozygous *gl6-ref* mutant and *Mu*-active lines; these mutants were designated *gl6-2*, *gl6-3*, *gl6-4*, and *gl6-5* (see Supplementary Table S1). An EMS mutagenesis screen identified three glossy mutants that were verified to be allelic to *gl6-ref*, and which were termed *gl6-6*, *gl6-7*, and *gl6-8* (Supplementary Table S1).

One *Mu*-tagged allele, *gl6-2*, was used to perform Seq-Walking sequencing, a genome walking approach to amplify and isolate DNA fragments flanking *Mu* transposon insertions throughout the genome (Li *et al.*, 2013). In total, 28 non-redundant *Mu* flanking sequence (MFS) sites with >30 reads were identified in the 18.9 Mb BSR-Seq mapping interval, and one *Mu*-insertion hotspot gene, GRMZM2G139786, containing three MFSs was identified (see Supplementary Fig. S1; Supplementary Table S2). At the same time, the *gl6-2* allele was also subjected to DLA analysis, an adaptor-mediated PCR-based method for isolating *Mu* flanking sequences that co-segregated with mutant phenotypes (Liu *et al.*, 2009). The DLA result independently identified a *Mu* insertion in GRMZM2G139786 that co-segregated with the *gl6* glossy phenotype (Fig. 5B). Based on these results, all four *Mu*-derived alleles, *gl6-2*, *gl6-3*, *gl6-4*, and *gl6-5*, were sequenced to identify mutations in GRMZM2G139786. *Mu1* insertions were identified 37 bp upstream of the *gl6* start codon in the *gl6-2* allele, 211 bp upstream of the start codon in both *gl6-4* and *gl6-5* alleles (Dietrich *et al.*, 2002), and 320 bp downstream of the start codon in the *gl6-3* allele (Fig. 5C).

The genomic sequences of GRMZM2G139786 from three EMS-induced *gl6* alleles were amplified and Sanger sequenced (see Supplementary Table S1). These analyses showed that the *gl6-6* allele contained a G to A transition 314 bp downstream of the start codon, producing a premature termination codon (PTC); *gl6-7* carried a C to T transition 391 bp downstream of

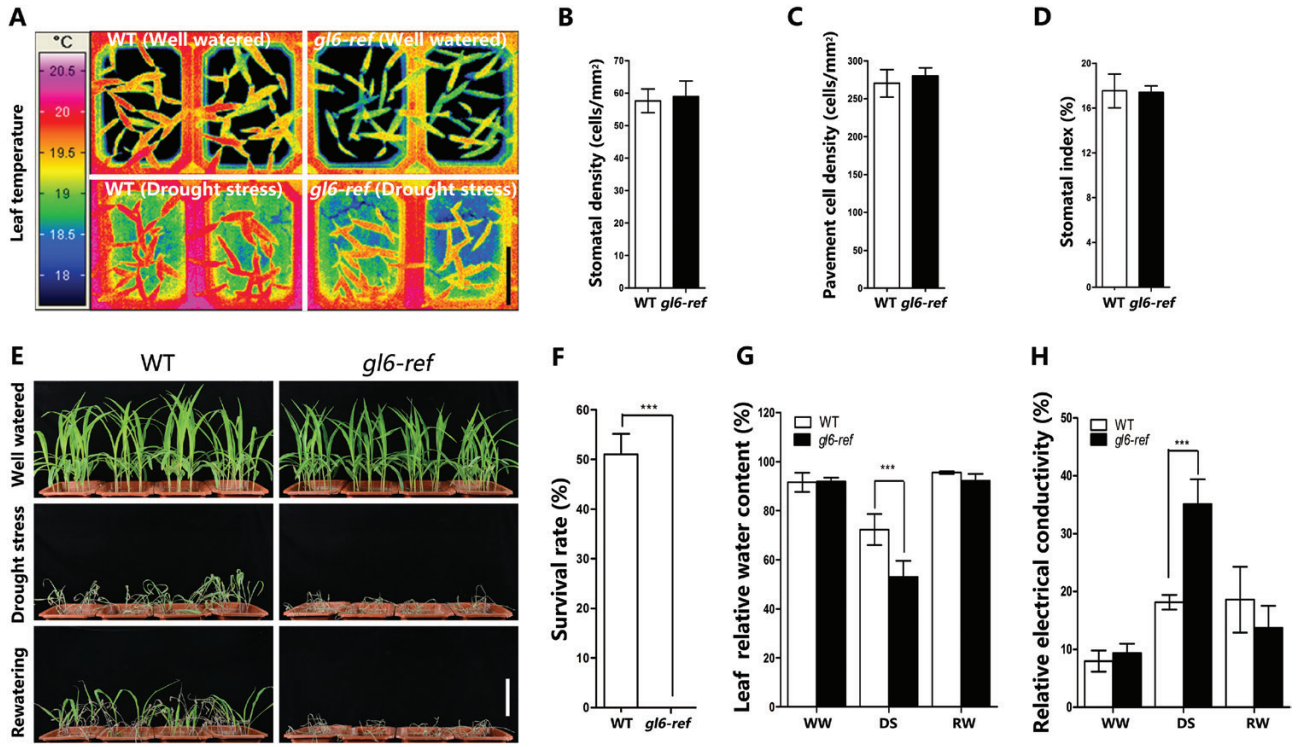

Fig. 4. *gl6-ref* mutant seedlings are sensitive to drought stress. (A) False-color infrared image of the wild-type and the *gl6-ref* mutant under well-watered and drought stressed conditions. (B–D) Stomatal density (B), pavement cell density (C), and stomatal index (number of stomata per total epidermal cells) (D) analysed in leaf abaxial epidermal layers from WT and *gl6-ref* mutant. Data are means of five individual plants. (E) Drought phenotypes of WT and *gl6-ref* mutant seedlings in soil following drought stress and after re-watering. (F) The survival rate of WT and *gl6-ref* mutant seedlings after drought stress and re-watering. (G, H) The leaf relative water content and relative electrical conductivity of WT and *gl6-ref* mutant seedlings under well-watered (WW), drought stressed (DS) and re-watered (RW) conditions. In (B–D, F), data are means of five replicates ±SD, and in (G, H) data are means of three replicates ±SD (***P<0.001, Student's t-test). Scale bars: 10 cm in (A, E). (This figure is available in color at *JXB* online.)

the start codon, causing an amino acid change from arginine to cysteine; and the *gl6-8* allele contained a 9-bp deletion 497 bp downstream of the start codon and seven non-synonymous mutations in the coding region (Supplementary Table S1; Fig. 5C). In addition, based on the BSR-Seq result, the accumulation of the GRMZM2G139786 transcripts was significantly reduced in the *gl6-ref* mutant pool as compared with the wild-type pool (Supplementary Table S3). Collectively, these results demonstrate that GRMZM2G139786 is the *gl6* gene.

Characterization of the novel glossy gene, gl6

The *gl6* gene has a single exon with a 675-bp open reading frame and encodes a putative protein with 224 amino acids. Domain analysis showed that GL6 is a novel protein containing a conserved DUF538 (domain of unknown function) between positions 29 and 138 aa of the protein (see Supplementary Fig. S2). Homologs of GL6 can be identified in sorghum, rice, Arabidopsis, and other plants. Phylogenetic analysis using the full-length protein sequences of GL6 homologs showed that GL6 was grouped into a monocot-specific subfamily (Fig. 5D), and multiple sequence alignment showed that the DUF538 domain of these proteins is highly conserved (Supplementary Fig. S2).

A fusion construct of GL6 with C-terminal YFP was generated and expressed in maize protoplast cells. Observation via confocal microscopy showed that GL6–YFP fluorescence signals were detected in the cytoplasm and the plasma membrane, but not in the nucleus, whereas the control YFP signal was observed throughout the cell (Fig. 6A, B). To further study the compartmental localization of the GL6 protein, we co-expressed GL6–YFP with the ER marker red fluorescent protein (RFP)–CNX, the Golgi marker mRFP–ManI, the *trans*-Golgi network (TGN) marker RFP–SYP41 and the nuclear protein marker mRFP–AHL22 in the protoplast cells, and the results revealed that GL6–YFP co-localized with the ER, Golgi, and TGN markers (Fig. 6C–E), but not with the nuclear protein marker (see Supplementary Fig. S3). To confirm plasma membrane localization of GL6, the GL6–YFP-expressing cells were incubated with the plasma membrane marker FM4-64, and the result showed that the signals of GL6–YFP and FM4-64 co-localized as expected (Fig. 6F). Together, our evidence indicated that GL6 is an ER membrane-, Golgi-, TGN-, and plasma membrane-localized protein.

gl6 *expression and transcriptome analysis of the* gl6 *mutant*

Real-time quantitative RT-PCR analysis was performed to detect *gl6* gene expression in different maize tissues, and the results showed that *gl6* was significantly expressed in leaves and silk, especially in young leaf, but there was lower expression in root, husk, anther, and immature seed (see Supplementary Fig. S4). To further understand the impact of the *gl6* mutation on

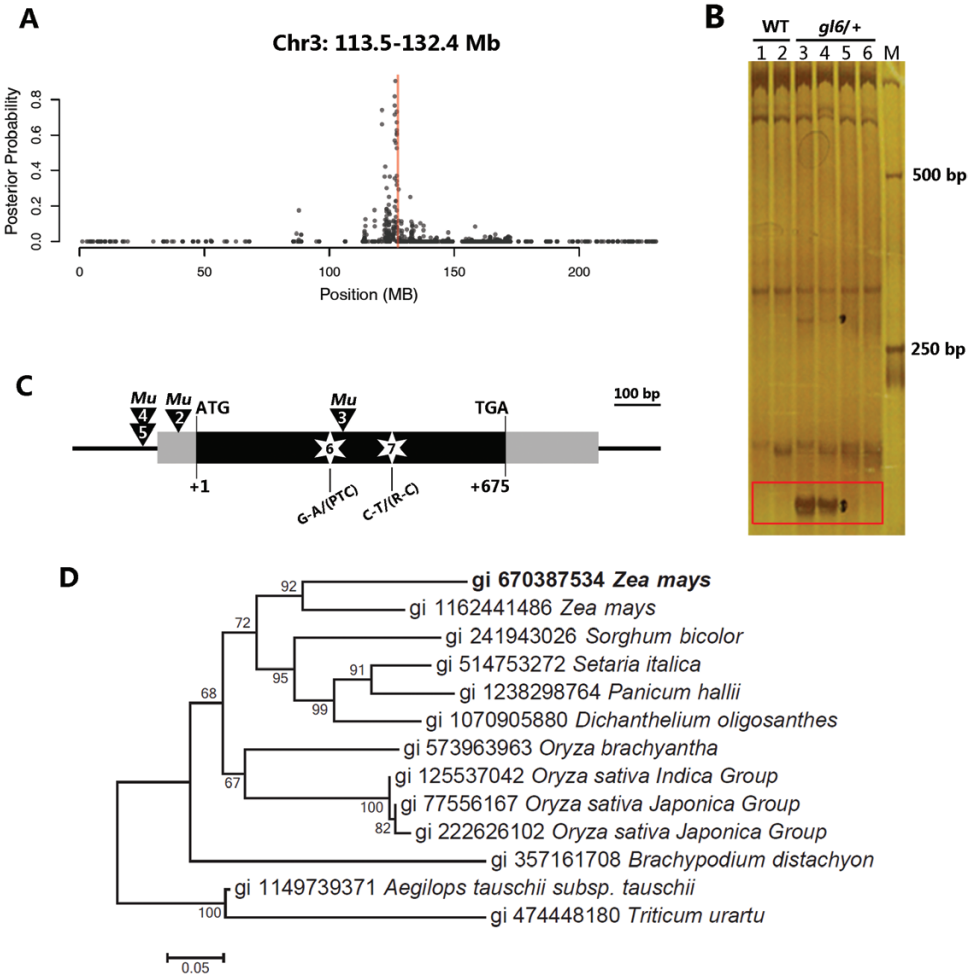

Fig. 5. Molecular cloning of the *gl6* gene and its phylogenetic analysis. (A) BSR-Seq analysis of an F_2 segregated *gl6-ref* population mapped *gl6* to the 113.5–132.4 Mb interval of chr3. (B) PAGE results of digestion–ligation–amplification (DLA) analysis using the adaptor primer (Nsp-15ctc). The rectangle indicates the specific bands produced from *gl6*/+ plants but not from WT plants. (C) The gene structure of *gl6*, *Mu* insertions in four alleles, and lesions in two *gl6* EMS alleles. (D) Phylogenetic tree constructed using MEGA 7.0 and the GL6 protein and GL6 homologs aligned using ClustalW. Distances were estimated with a neighbor-joining algorithm, and bootstrap support is indicated to the left of branches. (This figure is available in color at *JXB* online.)

the transcriptome, we analysed differential expression in the *gl6* mutant and wild-type using the BSR-Seq data. With a 10% false discovery rate, 421 differentially expressed (DE) genes were identified (Supplementary Table S4). Among the DE genes, 235 and 186 genes were up- and down-regulated in the *gl6* mutant versus wild-type, respectively (Supplementary Fig. S5A). Among the 235 up-regulated or 186 down-regulated genes, 197 (84%) and 135 (73%) genes exhibited greater than 2-fold changes. Gene Ontology (GO) enrichment analysis was performed on these DE genes using AgriGO (Du *et al.*, 2010), and complete lists of significantly enriched GO terms are shown in Supplementary Table S4. Significant enrichment of cellular response to stimulus and stress, especially to water and heat stresses, were observed among the enriched GO terms (Supplementary Fig. S5B), which is consistent with the hypothesis that the reduced wax accumulation on *gl6* leaves results in increased sensitivity to stimuli and stresses. Moreover, an enrichment of GO terms related to the fatty acid biosynthetic process was also observed. Of genes in these GO terms, two genes, GRMZM2G029912 and GRMZM2G083526, which are homologs of the Arabidopsis *CER3/WAX2* gene (AT5G57800) involved in the biosynthesis of VLCFAs, and another gene, GRMZM2G031790, a homolog of the Arabidopsis *KCS2* gene (AT1G04220), showed significantly higher expression in the *gl6* mutant with 12.0-, 4.8- and 12.5-fold changes, respectively (Lee *et al.*, 2009; Bernard *et al.*, 2012; Supplementary Table S3). This result suggested that altering wax amount and localization in the *gl6* mutant resulted in feedback, causing up-regulation of some genes in the fatty acid biosynthesis pathway.

Discussion

In this study, multiple strategies were combined to facilitate the genetic mapping and identification of a *gl6* candidate gene, which was confirmed using multiple independent *Mu*-tagged and EMS-induced *gl6* alleles. *gl6* is a novel gene with a conserved uncharacterized domain, opening the door to extending our understanding of the molecular basis of cuticular wax accumulation.

The phenotype and physiological characterization of the *gl6* mutant showed that *gl6* is a typical maize glossy mutant

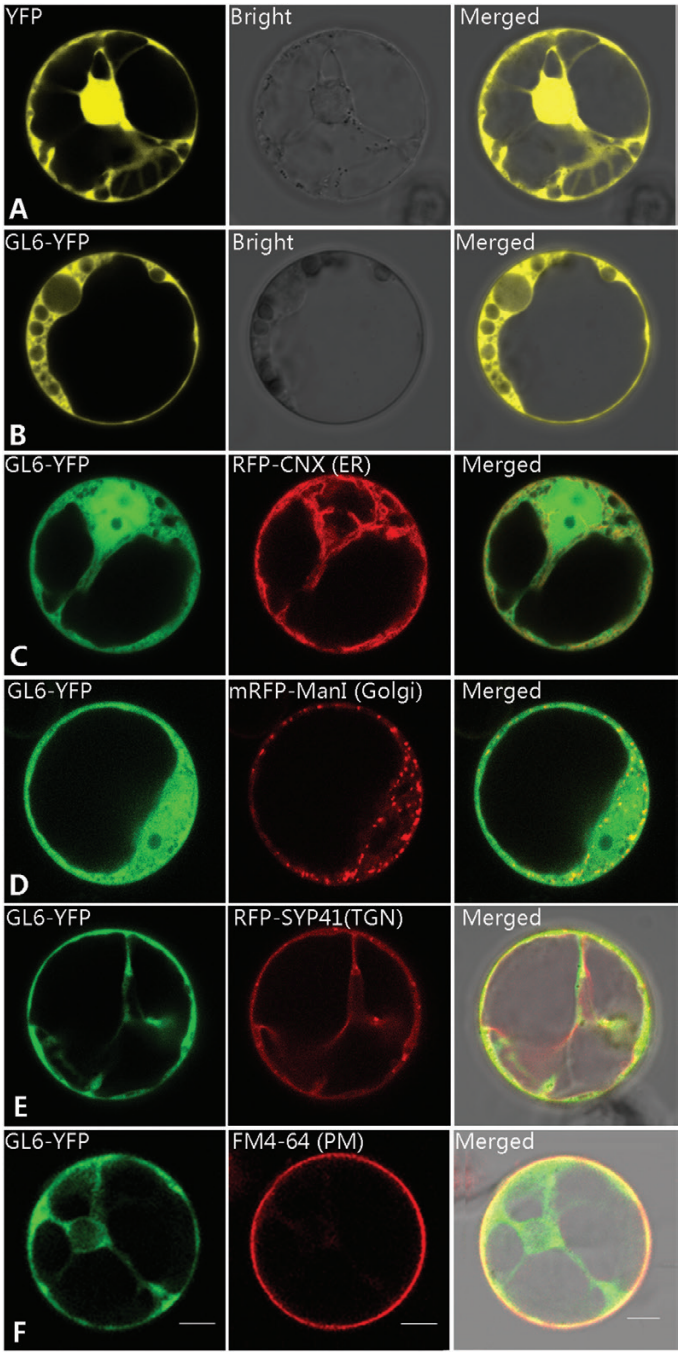

Fig. 6. Subcellular localization of the GL6 protein in maize protoplasts. Confocal images show the expression of YFP, GL6 fused at its C terminus with YFP, and organelle markers. (A, B) Subcellular localization YFP and GL6–YFP. (C) Co-localization of GL6–YFP with RFP–CNX (an ER marker). (D) Co-localization of GL6–YFP with mRFP–ManI (a Golgi marker). (E) Co-localization of GL6–YFP with RFP–SYP41 (a TGN marker). (F) Co-localization of GL6–YFP with FM4-64 (a plasma membrane marker). Scale bar: 10 μm. (This figure is available in color at *JXB* online.)

with reduced epicuticular wax accumulation on the leaf surface (Figs 1, 3). The amount of total cutin monomer present in *gl6-ref* mutant and wild-type seedling leaves was also examined, but no significant differences were detected, which indicates that the role of the *gl6* gene is specific to epicuticular waxes. Cuticular waxes, the hydrophobic layer on plant surfaces, protect leaves from non-stomatal water loss (Samuels *et al.*, 2008). However, few studies provide quantitative data to measure drought tolerance of maize glossy mutants. We demonstrated that the reduction of epicuticular waxes in the *gl6* mutant was associated with increased cuticle permeability and reduced drought tolerance of maize seedlings (Figs 3A, 4E). Studies from other plant species have shown that increases in cuticular wax load can enhance drought tolerance (Lü *et al.*, 2012; Luo *et al.*, 2013; Zhou *et al.*, 2013; Zhu and Xiong, 2013; Al-Abdallat *et al.*, 2014). Future studies should test the impact of elevated expression of cuticular wax on plant drought tolerance in adult maize plants as well as the potential physiological cost of accumulating abundant cuticular waxes.

Sequence analysis revealed that *gl6* encodes a novel protein containing a conserved DUF538 domain with no defined function (Supplementary Fig. S2). *gl6* orthologs were identified in sorghum, rice, Arabidopsis, and other plants, but none has been characterized. However, plant DUF538 proteins are predicted to be the potential homolog of mammalian BPI (bactericidal/permeability increasing) proteins (Gholizadeh and Kohnehrouz, 2013), which have been suggested to be important for the defense system against various pathogens (Srivastava *et al.*, 2007). Furthermore, BPI proteins are predicted to be structurally similar to esterase-type hydrolases, which implies DUF538 might have a lipid-associated enzymatic activity (Gholizadeh, 2014, 2016). The potential role of the *gl6* gene in wax transportation may result from the interaction of the GL6 protein with other transporters, as has been shown in other systems (Park *et al.*, 2013). In this study, we determined that maize *gl6* is involved in wax accumulation and drought tolerance, which will provide insights into understanding the molecular function of DUF538 family members in plants. It has been reported that the maize *gl1* mutant shows smaller and more densely arrayed trichomes (Sturaro *et al.*, 2005). Mutants of the Arabidopsis *gl1* homolog (*yre-1*) exhibit a wax-deficient phenotype that is associated with organ fusion and various abnormalities in trichome development (Kurata *et al.*, 2003). A T-DNA insertion mutation of the Arabidopsis *gl6* homolog, At1g56580, *svb-1*, exhibits smaller trichomes with variable branches as compared with wild-type (Marks *et al.*, 2009). However, no phenotype associated with cuticular wax accumulation has been reported for the *svb-1* mutant.

The *gl6* gene encodes a novel protein. Our characterizations have provided clues as to its function. VLCFAs are synthesized in the ER but the processes by which wax components from the ER are delivered to the plasma membrane remain unknown. Two hypotheses have been proposed, a Golgi-mediated vesicular trafficking pathway and transfers via physical ER–PM connections (Kunst and Samuels, 2003; Schulz and Frommer, 2004). Two vesicle-trafficking genes, *GNL1* and *ECH*, have been implicated in wax transport from the ER to the PM (McFarlane *et al.*, 2014), which supports the Golgi-mediated vesicular trafficking hypothesis. In the current study, the GL6 protein was localized in the ER membrane, the Golgi, the TGN, and the plasma membrane (Fig. 6), which provides further support for the involvement of the Golgi in intracellular wax transport. Our results also suggested that GL6 might play a role in the process of extracellular wax transport. Quantification of secreted waxes on the leaf surface and total

leaf waxes showed that a decrease of total waxes in the mutant was largely attributable to reduced accumulation of surface waxes (Table 1). Ignoring surface waxes, the remaining wax accumulation in mutants was higher than that in wild-type, indicative of dysfunctional wax export to leaf surfaces in the *gl6* mutant. Linear inclusions found in epidermal cells of the *gl6* mutant via TEM analysis provided further evidence that waxes accumulate inside epidermal cells of the *gl6* mutant (Fig. 1E). Taken together, our results suggest that GL6 functions in the intracellular transport of cuticular waxes, thereby influencing cuticular wax accumulation.

Supplementary data

Supplementary data are available at *JXB* online.

Fig. S1. *Mu* insertion sites from Seq-Walking.

Fig. S2. Multiple sequence alignment of amino acid sequences of the predicted maize GL6 protein and its homologs in other species.

Fig. S3. Co-localization of GL6–YFP with mRFP–AHL22 (nuclear marker).

Fig. S4. Accumulation of *gl6* transcripts in various tissues.

Fig. S5. Summary of DE genes and GO analysis.

Table S1. *gl6* allele information and the corresponding mutation types.

Table S2. *Mu* flanking sequences and *Mu* sequences for each *gl6 Mu* tagging allele.

Table S3. Differentially expressed genes in *gl6* mutant versus wild-type.

Table S4. Enriched GO terms in *gl6* mutant differentially expressed genes.

Acknowledgements

This work was supported by the National Key Research and Development Program of China (Grant No. 2016YFD0101002), the 948 project of the Ministry of Agriculture of China (Grant No. 2015-Z11), the Agricultural Science and Technology Innovation Program of CAAS, the National Natural Science Foundation of China (31701437), Iowa State University, and the Kansas Agricultural Experiment Station of Kansas State University. We thank Mr Cheng-Ting 'Eddy' Yeh, Drs Wei Wu, Heng-Cheng Hu and An-Ping Hsia for technical support and helpful discussions, Ms Mitzi Wilkening (ISU Genomic Technologies Facility) for sequencing services, former members of the Schnable lab including Philip Stinard and the late Joel Hansen, and the Schnable Lab's current nursery manager, Ms Lisa Coffey, for the generation and maintenance of genetic stocks used in this study. We thank Dr Jianxin Shi, Dr Guorun Qu, and Ms Qian Luo from Shanghai Jiao Tong University for their assistance in conducting the GC-FID and GC-MS measurements and associated data analyses.

References

Aharoni A, Dixit S, Jetter R, Thoenes E, van Arkel G, Pereira A. 2004. The SHINE clade of AP2 domain transcription factors activates wax biosynthesis, alters cuticle properties, and confers drought tolerance when overexpressed in *Arabidopsis*. The Plant Cell **16**, 2463–2480.

Al-Abdallat AM, Al-Debei HS, Ayad JY, Hasan S. 2014. Over-expression of *SlSHN1* gene improves drought tolerance by increasing cuticular wax accumulation in tomato. International Journal of Molecular Sciences **15**, 19499–19515.

Anders S, Pyl PT, Huber W. 2015. HTSeq—a Python framework to work with high-throughput sequencing data. Bioinformatics **31**, 166–169.

Bernard A, Domergue F, Pascal S, Jetter R, Renne C, Faure JD, Haslam RP, Napier JA, Lessire R, Joubès J. 2012. Reconstitution of plant alkane biosynthesis in yeast demonstrates that *Arabidopsis* ECERIFERUM1 and ECERIFERUM3 are core components of a very-long-chain alkane synthesis complex. The Plant Cell **24**, 3106–3118.

Bernard A, Joubès J. 2013. Arabidopsis cuticular waxes: advances in synthesis, export and regulation. Progress in Lipid Research **52**, 110–129.

Bessire M, Chassot C, Jacquat AC, Humphry M, Borel S, Petétot JM, Métraux JP, Nawrath C. 2007. A permeable cuticle in *Arabidopsis* leads to a strong resistance to *Botrytis cinerea*. The EMBO Journal **26**, 2158–2168.

Bird D, Beisson F, Brigham A, Shin J, Greer S, Jetter R, Kunst L, Wu X, Yephremov A, Samuels L. 2007. Characterization of Arabidopsis ABCG11/WBC11, an ATP binding cassette (ABC) transporter that is required for cuticular lipid secretion. The Plant Journal **52**, 485–498.

Candela H, Hake S. 2008. The art and design of genetic screens: maize. Nature Reviews. Genetics **9**, 192–203.

Chen W, Yu XH, Zhang K, Shi J, De Oliveira S, Schreiber L, Shanklin J, Zhang D. 2011. *Male Sterile2* encodes a plastid-localized fatty acyl carrier protein reductase required for pollen exine development in Arabidopsis. Plant Physiology **157**, 842–853.

Chen X, Goodwin SM, Boroff VL, Liu X, Jenks MA. 2003. Cloning and characterization of the WAX2 gene of *Arabidopsis* involved in cuticle membrane and wax production. The Plant Cell **15**, 1170–1185.

Chen X, Huang Q, Zhang F, Wang B, Wang J, Zheng J. 2014. ZmCIPK21, a maize CBL-interacting kinase, enhances salt stress tolerance in *Arabidopsis thaliana*. International Journal of Molecular Sciences **15**, 14819–14834.

Cui Y, Zhao Q, Gao C, Ding Y, Zeng Y, Ueda T, Nakano A, Jiang L. 2014. Activation of the Rab7 GTPase by the MON1-CCZ1 complex is essential for PVC-to-vacuole trafficking and plant growth in *Arabidopsis*. The Plant Cell **26**, 2080–2097.

Debono A, Yeats TH, Rose JK, Bird D, Jetter R, Kunst L, Samuels L. 2009. *Arabidopsis* LTPG is a glycosylphosphatidylinositol-anchored lipid transfer protein required for export of lipids to the plant surface. The Plant Cell **21**, 1230–1238.

Dietrich CR, Cui F, Packila ML, Li J, Ashlock DA, Nikolau BJ, Schnable PS. 2002. Maize *Mu* transposons are targeted to the 5′ untranslated region of the *gl8* gene and sequences flanking *Mu* target-site duplications exhibit nonrandom nucleotide composition throughout the genome. Genetics **160**, 697–716.

Dietrich CR, Perera MA, D Yandeau-Nelson M, Meeley RB, Nikolau BJ, Schnable PS. 2005. Characterization of two GL8 paralogs reveals that the 3-ketoacyl reductase component of fatty acid elongase is essential for maize (*Zea mays* L.) development. The Plant Journal **42**, 844–861.

Du Z, Zhou X, Ling Y, Zhang Z, Su Z. 2010. agriGO: a GO analysis toolkit for the agricultural community. Nucleic Acids Research **38**, W64–W70.

Earley KW, Haag JR, Pontes O, Opper K, Juehne T, Song K, Pikaard CS. 2006. Gateway-compatible vectors for plant functional genomics and proteomics. The Plant Journal **45**, 616–629.

Emerson RA, Beadle GW, Fraser AC. 1935. A summary of linkage studies in maize. Cornell University Agricultural Experiment Station Memoir **180**, 1–83.

Gholizadeh A. 2014. Prediction of tertiary structure homology between bactericidal/permeability increasing protein of innate immune system and hydrolase enzymes. International Journal of Biosciences **5**, 1–6.

Gholizadeh A. 2016. DUF538 protein superfamily is predicted to be chlorophyll hydrolyzing enzymes in plants. Physiology and Molecular Biology of Plants **22**, 77–85.

Gholizadeh A, Kohnehrouz SB. 2013. DUF538 protein super family is predicted to be the potential homologue of bactericidal/permeability-increasing protein in plant system. The Protein Journal **32**, 163–171.

Hansen JD, Pyee J, Xia Y, Wen TJ, Robertson DS, Kolattukudy PE, Nikolau BJ, Schnable PS. 1997. The glossy1 locus of maize and an epidermis-specific cDNA from *Kleinia odora* define a class of receptor-like proteins required for the normal accumulation of cuticular waxes. Plant Physiology **113**, 1091–1100.

Javelle M, Vernoud V, Depège-Fargeix N, Arnould C, Oursel D, Domergue F, Sarda X, Rogowsky PM. 2010. Overexpression of the epidermis-specific homeodomain-leucine zipper IV transcription factor Outer Cell Layer1 in maize identifies target genes involved in lipid metabolism and cuticle biosynthesis. Plant Physiology **154**, 273–286.

Kerstiens G. 1996. Cuticular water permeability and its physiological significance. Journal of Experimental Botany **47**, 1813–1832.

Kim D, Pertea G, Trapnell C, Pimentel H, Kelley R, Salzberg SL. 2013. TopHat2: accurate alignment of transcriptomes in the presence of insertions, deletions and gene fusions. Genome Biology **14**, R36.

Kosma DK, Bourdenx B, Bernard A, Parsons EP, Lü S, Joubès J, Jenks MA. 2009. The impact of water deficiency on leaf cuticle lipids of Arabidopsis. Plant Physiology **151**, 1918–1929.

Kunst L, Samuels AL. 2003. Biosynthesis and secretion of plant cuticular wax. Progress in Lipid Research **42**, 51–80.

Kunst L, Samuels L. 2009. Plant cuticles shine: advances in wax biosynthesis and export. Current Opinion in Plant Biology **12**, 721–727.

Kurata T, Kawabata-Awai C, Sakuradani E, Shimizu S, Okada K, Wada T. 2003. The *YORE-YORE* gene regulates multiple aspects of epidermal cell differentiation in *Arabidopsis*. The Plant Journal **36**, 55–66.

Lee SB, Jung SJ, Go YS, Kim HU, Kim JK, Cho HJ, Park OK, Suh MC. 2009. Two Arabidopsis 3-ketoacyl CoA synthase genes, *KCS20* and *KCS2/DAISY*, are functionally redundant in cuticular wax and root suberin biosynthesis, but differentially controlled by osmotic stress. The Plant Journal **60**, 462–475.

Lee SB, Suh MC. 2013. Recent advances in cuticular wax biosynthesis and its regulation in *Arabidopsis*. Molecular Plant **6**, 246–249.

Lee SB, Suh MC. 2015. Advances in the understanding of cuticular waxes in *Arabidopsis thaliana* and crop species. Plant Cell Reports **34**, 557–572.

Lemieux B. 1996. Molecular genetics of epicuticular wax biosynthesis. Trends in Plant Science **1**, 312–318.

Li L, Li D, Liu S, *et al*. 2013. The maize *glossy13* gene, cloned via BSR-Seq and Seq-walking encodes a putative ABC transporter required for the normal accumulation of epicuticular waxes. PLoS One **8**, e82333.

Liu S, Dietrich CR, Schnable PS. 2009. DLA-based strategies for cloning insertion mutants: cloning the *gl4* locus of maize using *Mu* transposon tagged alleles. Genetics **183**, 1215–1225.

Liu S, Yeh CT, Tang HM, Nettleton D, Schnable PS. 2012. Gene mapping via bulked segregant RNA-Seq (BSR-Seq). PLoS One **7**, e36406.

Livak KJ, Schmittgen TD. 2001. Analysis of relative gene expression data using real-time quantitative PCR and the $2^{-\Delta\Delta C^T}$ method. Methods **25**, 402–408.

Love MI, Huber W, Anders S. 2014. Moderated estimation of fold change and dispersion for RNA-seq data with DESeq2. Genome Biology **15**, 550.

Lü S, Zhao H, Des Marais DL, *et al*. 2012. Arabidopsis *ECERIFERUM9* involvement in cuticle formation and maintenance of plant water status. Plant Physiology **159**, 930–944.

Luo X, Bai X, Sun X, *et al*. 2013. Expression of wild soybean WRKY20 in Arabidopsis enhances drought tolerance and regulates ABA signalling. Journal of Experimental Botany **64**, 2155–2169.

Marks MD, Wenger JP, Gilding E, Jilk R, Dixon RA. 2009. Transcriptome analysis of *Arabidopsis* wild-type and *gl3–sst sim* trichomes identifies four additional genes required for trichome development. Molecular Plant **2**, 803–822.

McFarlane HE, Watanabe Y, Yang W, Huang Y, Ohlrogge J, Samuels AL. 2014. Golgi- and trans-Golgi network-mediated vesicle trafficking is required for wax secretion from epidermal cells. Plant Physiology **164**, 1250–1260.

Moose SP, Sisco PH. 1996. *Glossy15*, an APETALA2-like gene from maize that regulates leaf epidermal cell identity. Genes & Development **10**, 3018–3027.

Murray MG, Thompson WF. 1980. Rapid isolation of high molecular weight plant DNA. Nucleic Acids Research **8**, 4321–4325.

Mustilli AC, Merlot S, Vavasseur A, Fenzi F, Giraudat J. 2002. Arabidopsis OST1 protein kinase mediates the regulation of stomatal aperture by abscisic acid and acts upstream of reactive oxygen species production. The Plant Cell **14**, 3089–3099.

Nadakuduti SS, Pollard M, Kosma DK, Allen C Jr, Ohlrogge JB, Barry CS. 2012. Pleiotropic phenotypes of the *sticky peel* mutant provide new insight into the role of *CUTIN DEFICIENT2* in epidermal cell function in tomato. Plant Physiology **159**, 945–960.

Nawrath C. 2006. Unraveling the complex network of cuticular structure and function. Current Opinion in Plant Biology **9**, 281–287.

Negruk V, Yang P, Subramanian M, McNevin JP, Lemieux B. 1996. Molecular cloning and characterization of the *CER2* gene of *Arabidopsis thaliana*. The Plant Journal **9**, 137–145.

Park S, Gidda SK, James CN, Horn PJ, Khuu N, Seay DC, Keereetaweep J, Chapman KD, Mullen RT, Dyer JM. 2013. The α/β hydrolase CGI-58 and peroxisomal transport protein PXA1 coregulate lipid homeostasis and signaling in *Arabidopsis*. The Plant Cell **25**, 1726–1739.

Pighin JA, Zheng H, Balakshin LJ, Goodman IP, Western TL, Jetter R, Kunst L, Samuels AL. 2004. Plant cuticular lipid export requires an ABC transporter. Science **306**, 702–704.

Samuels L, Kunst L, Jetter R. 2008. Sealing plant surfaces: cuticular wax formation by epidermal cells. Annual Review of Plant Biology **59**, 683–707.

Schnable PS, Stinard PS, Wen TJ, Heinen S, Weber D, Zhang L, Hansen JD, Nikolau BJ. 1994. The genetics of cuticular wax biosynthesis. Maydica **39**, 279–287.

Schulz B, Frommer WB. 2004. Plant biology. A plant ABC transporter takes the lotus seat. Science **306**, 622–625.

Shepherd T, Wynne Griffiths D. 2006. The effects of stress on plant cuticular waxes. New Phytologist **171**, 469–499.

Srivastava A, Casey H, Johnson N, Levy O, Malley R. 2007. Recombinant bactericidal/permeability-increasing protein rBPI21 protects against pneumococcal disease. Infection and Immunity **75**, 342–349.

Sturaro M, Hartings H, Schmelzer E, Velasco R, Salamini F, Motto M. 2005. Cloning and characterization of *GLOSSY1*, a maize gene involved in cuticle membrane and wax production. Plant Physiology **138**, 478–489.

Tacke E, Korfhage C, Michel D, Maddaloni M, Motto M, Lanzini S, Salamini F, Döring HP. 1995. Transposon tagging of the maize *Glossy2* locus with the transposable element *En/Spm*. The Plant Journal **8**, 907–917.

Xiao C, Chen F, Yu X, Lin C, Fu YF. 2009. Over-expression of an AT-hook gene, *AHL22*, delays flowering and inhibits the elongation of the hypocotyl in *Arabidopsis thaliana*. Plant Molecular Biology **71**, 39–50.

Xu X, Dietrich CR, Delledonne M, Xia Y, Wen TJ, Robertson DS, Nikolau BJ, Schnable PS. 1997. Sequence analysis of the cloned *glossy8* gene of maize suggests that it may code for a beta-ketoacyl reductase required for the biosynthesis of cuticular waxes. Plant Physiology **115**, 501–510.

Xue D, Zhang X, Lu X, Chen G, Chen ZH. 2017. Molecular and evolutionary mechanisms of cuticular wax for plant drought tolerance. Frontiers in Plant Science **8**, 621.

Zhang Z, Wei W, Zhu H, Challa GS, Bi C, Trick HN, Li W. 2015. W3 is a new wax locus that is essential for biosynthesis of β-diketone, development of glaucousness, and reduction of cuticle permeability in common wheat. PLoS One **10**, e0140524.

Zheng J, Fu J, Gou M, *et al*. 2010. Genome-wide transcriptome analysis of two maize inbred lines under drought stress. Plant Molecular Biology **72**, 407–421.

Zhou L, Ni E, Yang J, Zhou H, Liang H, Li J, Jiang D, Wang Z, Liu Z, Zhuang C. 2013. Rice OsGL1-6 is involved in leaf cuticular wax accumulation and drought resistance. PLoS One **8**, e65139.

Zhu X, Xiong L. 2013. Putative megaenzyme DWA1 plays essential roles in drought resistance by regulating stress-induced wax deposition in rice. Proceedings of the National Academy of Sciences, USA **110**, 17790–17795.